Towards clinical significance prediction using k^{trans} evidences in prostate cancer

Yesid Gutiérrez , Gustavo Garzón, and Fabio Martínez

⋆ Biomedical Imaging, Vision and Learning Laboratory (BIVL^{2}ab)
Motion Analysis and Computer Vision (MACV)
Universidad Industrial de Santander (UIS)
Bucaramanga, Colombia

***Abstract*—Currently, K^{trans} coefficient maps have emerged to characterize tumor biology and treatment response. Salient localized coefficient on K^{trans} allows to detect and localize tumor regions from non-invasive MRI scanners. Nevertheless, such identified lesions on K^{trans} maps are highly variable and in much of the cases result in false positive indicators. In this work a set of labeled K^{trans} regions are processed into a supervised framework to correctly find true positive regions that are prostate cancer indicators. Three different algorithms were implemented to perform the classification: K-Nearest Neighbors (k-NN), Support vector machine (SVM), and Random forest (RaF). On a public dataset with 339 K^{trans} images on peripheral, transitional and anterior fibromuscular stroma regions, the SVM achieved an average accuracy of 80.83% with a ROC AUC of 0.68 on true evidence identification.**

***Index Terms*—Prostate cancer, Cancer detection, K^{trans} images, Machine learning.**

I. Introduction

Prostate cancer is the first on prevalence and the second on incidence of cancer worldwide for men, with percentages about 20.8 % and 14.5 % respectively. [1]. Regarding Colombia, prostate cancer is the first incidence and prevalence of cancer for men, reporting 27.043 cases diagnosed during 2018 [1]. Despite of recent advances on characterization and detection of this disease, the factors for the development and progression of the cancer remain unknown. Additionally, current techniques remain limited to carrying out a reliable early detection of cancer, together with a proper morphological tumor characterization.

During clinical routine, the diagnostic of prostate cancer is firstly carried out from a non-specific blood test named *prostate specific antigen (PSA)*. This test measures the level of glycoprotein present in a man's blood and is correlated with the disease [2]. However, PSA test presents low specificity ($\sim 25\%$) giving a lot of false positives for cancer detection and requiring additional exams to obtain a more accurate diagnosis [2]. A second step of disease characterization is performed by the digital rectal examination (DRE). This exam consist on a gloved finger insertion into the rectum to feel the prostate for hard, lumpy or abnormal areas to find abnormalities. However, DRE is limited to the physician's experience and thus, introduces an inter-expert variability on the diagnosis. In more specialized steps, a transrectal ultrasound (TRUS) guided biopsy is provided by taking samples of tissue from the prostate gland to analyze for cancer cells [3]. However, TRUS biopsy report about 30% of false negatives with some side effects such as: rectal bleeding, transurethral bleeding, bacteriuria and sepsis [4], [5].

Currently, Magnetic Resonance Imaging (MRI) has became an important tool for detection and characterization of prostate cancer [6], [7]. For instance, multi-parametric MRI (mp-MRI) can be helpful confirming the absence of significant intraprostatic disease [6] in low-risk patients. Also, (mp-MRI) can be a powerful tool, using a Dynamic Contrast Enhanced (DCE) procedure to analyze microcirculation in tissues related with nodal metastases [6], [8]. Specifically, K^{trans} images, pharmacokinetics DCE-MRI maps, have emerged to detect malign tumors on specific zones. These sequences provide information about the micro-circulation's physiological parameters such as extra-vascular and extracellular volume fraction (v_e), blood volume fraction (v_s) and blood flow (F_T) [9]. Such parameters could be used as potential markers to detect and quantify tumor angiogenesis [9]. However, the identification of malignant tumors is carried out by oncologist experts, and, in much of the cases, such evidences result in false positives because angiogenesis is confused with wound healing process [10], [11].

Hence, computational strategies result fundamental to characterize evidences marked on K^{trans} sequences and to assist with prostate cancer diagnosis and treatment. For instance, a multiparametric approach fussed different images modalities like T2-weighted images, Diffusion-Weighted Imaging (DWI) and DCE-MRI to automatically predict cancer, under a logistic regression classifier [12]. This approach was applied to periphereal zones but the classification approach has several limitation to detect true positive evidences. Also, Giannini et al. [13] proposed a computer-assisted diagnosis (CAD) for peripheral zone prostate cancer detection with a multiparametric endorectal MRI approach, with a SVM classifier. Niaf et al. [14] proposed a CAD system using T2-weighted, DCE-MRI and DWI images at the peripheral zone with a t-test feature selection and a SVM classifier. Despite the obtained results in these approaches, the use of multiple modalities limit its

application in real clinical scenarios.

This work introduced a fully evaluation of K^{trans} evidences as potential marker to automatically predict prostate cancer. For doing so, the proposed approach uses different prostate zones such as peripheral (PZ), transitional (TZ) and anterior fibromuscular stroma (AS). A set of expert annotations over K^{trans} maps, at different zones, are taken into account, bounded as 3d volume patches. This patches represent the K^{trans} descriptor that thereafter are mapped to machine learning classifiers. Several machine learning strategies were then implemented to evaluate K^{trans} evidences.

II. Materials

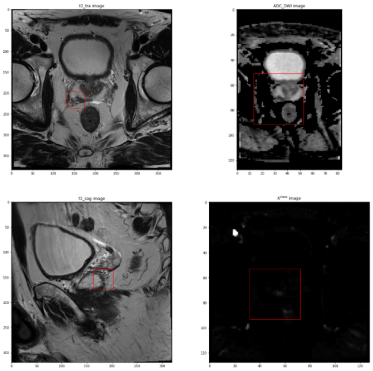

Fig. 1: Top: T2 weighted transaxial image (left), apparent diffusion coefficient image (right), Bottom: T2 weighted sagittal image (left), K^{trans} image (right).

A. K^{trans} Images

K^{trans} images have recently emerged as an alternative to characterize and follow cancer tumors. These images are captured from the Dynamic contrast-enhanced T1-weighted series, measuring the accumulation of gadolinium-based contrast in the extravascular extracellular space (EES) [15]. K^{trans} series represent a key pharmacokinetic parameter that depends on three main factors: plasma blood flow, vascular permeability and capillary surface area [8]. In addition, K^{trans} images have shown in previous studies a correlation with histopathologic grades of gliomas [16] [17].

In figure 1 (bottom-right) is illustrated a typical K^{trans} map, in which the highlighted zones represent high-permeability of blood plasma flow per unit volume of tissue. The morphological equivalence is captured in T2-weighed images illustrated at the figure 1 (top-left) and figure 1 (bottom-left), for axial and sagittal plane respectively. Figure 1 (top - right) shows an Apparent diffusion coefficient (ADC) image that measures the magnitude of diffusion of the water molecules within the tissue [18]. In addition, previous studies have shown a negative correlation between ADC and the Gleason grade group which is a scoring system that measures the aggressiveness of prostate cancer [19].

B. Data

The data used in this work was obtained from The Cancer Imaging Archive (TCIA) sponsored by the SPIE, NCI/NIH, AAPM, and Radboud University. The data-set contains 204 MRI cases for training and 142 MRI cases for testing, each case consists of four sets of MRI scan data: two sets of T2-weighted images, K^{trans} images (computed from dynamic contrast-enhanced (DCE) images), and apparent diffusion coefficient (ADC) images (computed from diffusion-weighted (DWI) imaging) [20].

The dataset includes findings that contain information about the $[i, j, k]$ Prostate's lesion position, the clinical significance (ClinSig), the identification of the patient (ProxID), the index of the finding (fid) and the prostate zone of the study, all of these findings were provided by expert radiologists [20]. Because of the goal of this work, only the subset of K^{trans} evidences were used to codify the descriptor and training the classifiers. K^{trans} images come with a shape of (16 slices, 128 rows and 128 columns) and only one K^{trans} image is provided per finding [20]. In this work, the dataset was divided into 3 sub-datasets in order to study the performance of each classifier per prostate zone, (peripheral data, transitional data and anterior fibromuscular stroma data).

III. Methods

A. 3D findings characterization

A set of labeled patches over K^{trans} images were computed as visual clinical significant descriptors. In such case, the salient pharmacokinetic point parameter marked by an expert as a candidate to be correlated with cancer disease was fixed as a reference to bound a volumetric region. In such sense, this region describes the excessive accumulation of gadolinium which could be related with tumor morphology.

Technically, given a K^{trans} volume $I \in \mathbb{R}^3$, coded as a set of stacked slices, was extracted a set of volumetric regions $\{\mathbf{x_1}, \mathbf{x_2}, \ldots, \mathbf{x_k}\}$. Each $\mathbf{x_i}$ is centered on location given by the expert (ClinSig). A bounded region $\mathbf{x_i}$ is then coded as a descriptor of the lesion, being the voxel intensity values the corresponding features. In this work was decided to fit raw voxels as features to effectively measure the corresponding sign with the disease.

B. Clinical significance prediction of the prostate lesion

The main goal of this work is to predict the value of the clinical significance $\hat{y_i} = \{0, 1\}$ (non-malignancy status and malignancy status respectively) to a given prostate lesion located at patch $\mathbf{x_i} \in R^{3*40*40}$, being $\mathbf{x_i} = [x_1, x_2, x_3, x_i, \ldots, x_k]$ a set of voxel values coded as features of the given prostate lesion. In this work was found that a region with $k = 4800$ scalar values have a proper trade-off between accuracy and computational cost for the classifiers. Formally, the training dataset used in this work can be described as follows:

$$L = \{(\mathbf{x_i}, y_i), i = 1, 2, 3, \ldots, N\}$$

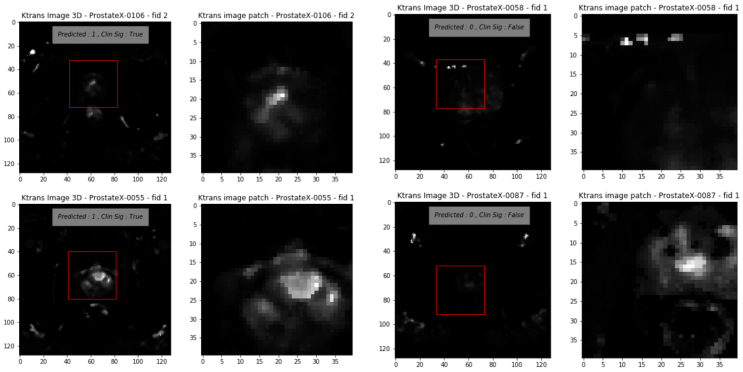

((a)) ((b))

Fig. 2: Left block ((a)): a sample of true positive K^{trans} patch images. Right block ((b)): a sample of true negative K^{trans} patch images.

Where N is the size of the dataset which corresponds to 339 labeled pairs $(\mathbf{x_i}, y_i)$ that were assigned as 60% for training and 40% for testing purposes.

The current work formulated the prediction as a binary classification problem. Likewise, non-linear classifier were selected to find better discrimination patterns from clinical evidences, coded as descriptors. Additional criteria for finding an adequate set of classification strategies were the reduced size of the dataset and how well a prediction could be explained from input descriptors. Since our method is intended to help on the diagnosis, it is desirable to understand how the prediction is performed. Therefore, machine learning algorithms were selected for the classification task: Random Forest (RAC), Support Vector Machine (SVM) and K-Nearest Neighbors (k-NN). In contrast, deep learning strategies need a massive amount of samples and the details of the classification process is namely unclear.

To prevent the effect of class imbalance, a couple of weight parameters $[W_0, W_1]$ were adjusted, in which $W_0 = 1$ and $W_1 = 1 + \frac{P}{P+F}$, where P be the number of samples for class $\{1\}$ at training and F the number of samples for class $\{0\}$.

C. Random forest findings predictions

A first selected classifier was the unsupervised, non-parametric and ensemble random forest approach (RFC). Given the set of training of ClinSig descriptors $\{\mathbf{x_1}, \mathbf{x_2}, \ldots, \mathbf{x_k}\}$, a set of random decision trees (DT) are built to predict independently cancer evidences. Each DT is built from a random selection of training features $\mathbf{x_i}$, following an uniform distribution with *i.i.d* properties. For each selected feature on training dataset, is learned a particular threshold τ_i that forms a node $\varrho(x_i, \tau_i)$ and produces a bi-partition on tree. This process is carried following a Gini impurity measure that counts the occurrence of random feature selection incorrectly labeled.

Hence, The random forest (RFC) classification consists on a set of decision tree classifiers, allowing to overcome sensibility problems of decision by taking mode decisions over the set of computed trees. In our specific approach, a set of twenty independent DT algorithms are trained over different 3D ClinSig descriptors $\mathbf{x}$. The final prediction may be carried out by averaging the predictions of individual trees f_b, or taking the majority vote as expressed : $\hat{y} = \frac{1}{B}\sum_{b=1}^{B} f_b \wedge \hat{y} = \arg\max\{f_1, \ldots f_B\}$.

D. Support Vector Machines findings predictions

The second classifier herein implemented was the Support Vector Machines (SVM). This classifier is widely recognized in pattern recognition tasks because of its ability to define boundaries from non-linear kernels. Hence, a SVM will calculate an optimal hyperplane that maximizes the distance of all samples with respect to such hyperplane. In order to facilitate calculations of the optimal hyperplane, a Radial Basis Function (RBF) kernel, that is: $K(x_i, x_j) = exp(-\gamma\|x_i - x_j\|^2)$ lead to non-linear class separations showing favorable results. In this case, $\|x_i - x_j\|^2$ is a Euclidean distance between different clinically significant features. This kernel has some interesting properties such as non local minima convergences. Also, the boundary description could be performed from a continuous function, resulting in stable prediction. In this work the SVM was implemented using LIBSVM library [21].

E. k-nearest neighbors to (K-NN) findings prediction

Finally, the k-nearest neighbors (K-NN) algorithm was herein considered for the task of clinically significant evidence classification. This non-parametric approach allows to assign a label to each new sample $\curvearrowleft\sqsupset$ according to the closest training samples. In this approach, each sample is classified by taking into account the vote of its neighbors, and is assigned to the class that is most frequent among their k nearest neighbors. Distance to each neighbor is given by the Euclidean distance, as: $d(\mathbf{x_m}, \mathbf{x_n}) = \sqrt{\sum_{r=1}^{n}(\mathbf{x_{rm}} - \mathbf{x_{rn}})^2}$. In our case, each sample $\mathbf{x_i}$ is classified taking into account twenty nearest neighbors [22]. A main advantage of this approach is the simplicity which imply computational efficiency to predict correlation evidences with prostate cancer. Additionally, the

computed prediction could be understood from the assigned neighbors that voted for a given class.

IV. Results

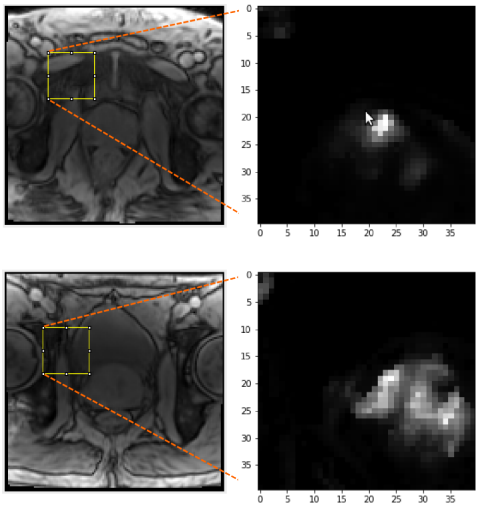

Fig. 3: Top: T1-weighted Fast Low Angle Shot (left) and a K^{trans} image patch (right) showing a true positive. Bottom: T1-weighted Fast Low Angle Shot (left) and a K^{trans} image patch (right) showing a false positive.

Evaluation in this work were carried out using visual clinically significant features collected from K^{trans} images, to understand the discriminative power of this MRI modality in automatic prediction computer-assisted diagnosis (CAD) systems. In Figure 3 is illustrated the complexity of this problem, in which a true positive and a false positive evidences were found for the same prostate zone, and looks quite identical on T1-weighted sequences. In such cases, a proper K^{trans} regional modelling could stand out different microcirculation behaviours and help with the correct prostate cancer diagnosis. This kind of examples are challenging even for expert radiologists that follow classical clinical protocols [8].

For quantitative results, a statistical K-fold validation was implemented, setting $K = 8$. The whole dataset of K^{trans} sequences were normalized and the classifier was optimized to obtain the best possible score. Table I summarizes the obtained result for different classifiers at different prostate zones. In general, three classifiers achieved a proper classification prediction of K^{trans} evidences, coded into volumetric and localized patches. As expected, peripheral (PZ) and transitional (TZ) zones had a better true positive identification because of the well defined morphology of tumor in this views. Nevertheless, the anterior Fibromuscular Stroma (AS) using RFC shows a interesting result that could be significant as a first step to support diagnosis. In spite of RFC having some salient results, the SVM achieved a more stable prediction, obtaining a lower standard deviation on their predictions.

Because SVM classifier achieved more stable results, an operating characteristic curve (ROC curve) was computed to

TABLE I: Results

Zones	Classifiers		
	RFC	***(k=20)-NN***	***SVM***
PZ	80.00 ±4.71	80.83 ±2.20	81.66 ±2.88
TZ	91.07 ±14.17	92.85 ±7.14	92.85 ±7.14
AS	62.91 ±19.90	60.41 ±9.92	57.91 ±6.65
ALL	75.89 ±6.66	76.83 ±3.68	80.83 ±3.82

Scores of an 8-fold cross validation using 20-Nearest Neighbors ((k=20)-NN), Support Vector Machine (SVM) and random forest classifiers (RFC) at peripheral zone (PZ), transitional zone (TZ), anterior fibromuscular stroma (AS) and all the zones together (ALL).

have a more detailed analysis. This curve represents sensitivity against recall or probability of detection. The metric used to quantify the results of each one of the ROC curves is the Area Under the Curve (AUC).

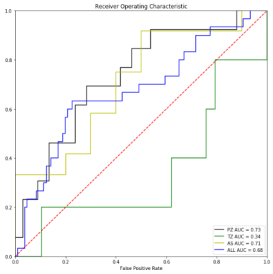

Fig. 4: ROC Curves of the SVM classifier reached an AUC of 0.73, 0.31, 0.71 and 0.68 at peripheral, transitional , anterior fibromuscular stroma and ALL zones respectively.

High values of AUC correspond to proper prediction of K^{trans} evidences, showing that for much of the prostate zones the SVM performed a correct validation. Low values of AUC correspond to false positives generated by angiogenesis which is not necessarily an indicator of a malignant tumor [10].

As presented, the goal of the project was to deeply evaluate the power of K^{trans} evidences as a biomarker for prostate cancer. In such sense, the three prostate zones were taken into account, resulting in notable differences of accuracy to detect correct evidences. In literature is namely only taking into account peripheral zone [13], [14], [23] because the predominant regions of the tumor but discarding important portion of carcinoma's origin sites [24].

V. Conclussion

In this work was introduced a MRI monoparametric approach that using a DCE K^{trans} pharmacokinetic is able to predict prostate cancer. This study result relevant to develop computer-assisted diagnosis (CAD) systems for intermediate-risk patients that report high probability of extra-prostatic spread rise. A set of visual K^{trans} volumetric evidences were coded as descriptors and mapped to three different non-linear classifiers. In general, computational classifiers demostrated a proper performance to support diagnosis, while regional evidences are directly correlated with disease.

ACKNOWLEDGEMENTS

This work was partially funded by the Universidad Industrial de Santander. The authors acknowledge the *Vicerrectoría de Investigación y Extensión (VIE)* of the Universidad Industrial de Santander for supporting this research registered by the project: *Reconocimiento continuo de expresiones cortas del lenguaje de señas registrado en secuencias de video*, with VIE code 1293.

REFERENCES

[1] J. Ferlay, M. Colombet, I. Soerjomataram, C. Mathers, D. Parkin, M. Piñeros, A. Znaor, and F. Bray, "Estimating the global cancer incidence and mortality in 2018: Globocan sources and methods," *International Journal of Cancer*, 2018.

[2] M. J. Barry, "Prostate-specific–antigen testing for early diagnosis of prostate cancer," *New England Journal of Medicine*, vol. 344, no. 18, pp. 1373–1377, 2001.

[3] D. Greene, A. Ali, N. Kinsella, *et al.*, "Transrectal ultrasound and prostatic biopsy: Guidelines & recommendations for training," 2015.

[4] H. U. Ahmed, A. El-Shater Bosaily, L. C. Brown, R. S. Kaplan, Y. Colaco-Moraes, K. Ward, R. G. Hindley, A. Freeman, A. K. Kirkham, R. Oldroyd, *et al.*, "The promis study: A paired-cohort, blinded confirmatory study evaluating the accuracy of multi-parametric mri and trus biopsy in men with an elevated psa.," 2016.

[5] M. Shahait, J. Degheili, F. El-Merhi, H. Tamim, and R. Nasr, "Incidence of sepsis following transrectal ultrasound guided prostate biopsy at a tertiary-care medical center in lebanon," *International braz j urol*, vol. 42, no. 1, pp. 60–68, 2016.

[6] J. O. Barentsz, J. Richenberg, R. Clements, P. Choyke, S. Verma, G. Villeirs, O. Rouviere, V. Logager, and J. J. Fütterer, "Esur prostate mr guidelines 2012," *European radiology*, vol. 22, no. 4, pp. 746–757, 2012.

[7] G. Murphy, M. Haider, S. Ghai, and B. Sreeharsha, "The expanding role of mri in prostate cancer," *American Journal of Roentgenology*, vol. 201, no. 6, pp. 1229–1238, 2013.

[8] C. Cuenod and D. Balvay, "Perfusion and vascular permeability: basic concepts and measurement in dce-ct and dce-mri," *Diagnostic and interventional imaging*, vol. 94, no. 12, pp. 1187–1204, 2013.

[9] S. Verma, B. Turkbey, N. Muradyan, A. Rajesh, F. Cornud, M. A. Haider, P. L. Choyke, and M. Harisinghani, "Overview of dynamic contrast-enhanced mri in prostate cancer diagnosis and management," *American Journal of Roentgenology*, vol. 198, no. 6, pp. 1277–1288, 2012.

[10] J. Penn, *Retinal and choroidal angiogenesis*. Springer Science & Business Media, 2008.

[11] J. Li, Y.-P. Zhang, and R. S. Kirsner, "Angiogenesis in wound repair: angiogenic growth factors and the extracellular matrix," *Microscopy research and technique*, vol. 60, no. 1, pp. 107–114, 2003.

[12] D. L. Langer, T. H. van der Kwast, A. J. Evans, J. Trachtenberg, B. C. Wilson, and M. A. Haider, "Prostate cancer detection with multi-parametric mri: Logistic regression analysis of quantitative t2, diffusion-weighted imaging, and dynamic contrast-enhanced mri," *Journal of Magnetic Resonance Imaging: An Official Journal of the International Society for Magnetic Resonance in Medicine*, vol. 30, no. 2, pp. 327–334, 2009.

[13] V. Giannini, S. Mazzetti, A. Vignati, F. Russo, E. Bollito, F. Porpiglia, M. Stasi, and D. Regge, "A fully automatic computer aided diagnosis system for peripheral zone prostate cancer detection using multi-parametric magnetic resonance imaging," *Computerized Medical Imaging and Graphics*, vol. 46, pp. 219–226, 2015.

[14] E. Niaf, O. Rouvière, F. Mège-Lechevallier, F. Bratan, and C. Lartizien, "Computer-aided diagnosis of prostate cancer in the peripheral zone using multiparametric mri," *Physics in Medicine & Biology*, vol. 57, no. 12, p. 3833, 2012.

[15] M. Essig, M. S. Shiroishi, T. B. Nguyen, M. Saake, J. M. Provenzale, D. Enterline, N. Anzalone, A. Dörfler, À. Rovira, M. Wintermark, *et al.*, "Perfusion mri: the five most frequently asked technical questions," *American Journal of Roentgenology*, vol. 200, no. 1, pp. 24–34, 2013.

[16] M. A. Blake and M. K. Kalra, *Imaging in oncology*, vol. 143. Springer Science & Business Media, 2008.

[17] N. Zhang, L. Zhang, B. Qiu, L. Meng, X. Wang, and B. L. Hou, "Correlation of volume transfer coefficient ktrans with histopathologic grades of gliomas," *Journal of Magnetic Resonance Imaging*, vol. 36, no. 2, pp. 355–363, 2012.

[18] R. Sener, "Diffusion mri: apparent diffusion coefficient (adc) values in the normal brain and a classification of brain disorders based on adc values," *Computerized medical imaging and graphics*, vol. 25, no. 4, pp. 299–326, 2001.

[19] T. Hambrock, D. M. Somford, H. J. Huisman, I. M. van Oort, J. A. Witjes, C. A. Hulsbergen-van de Kaa, T. Scheenen, and J. O. Barentsz, "Relationship between apparent diffusion coefficients at 3.0-t mr imaging and gleason grade in peripheral zone prostate cancer," *Radiology*, vol. 259, no. 2, pp. 453–461, 2011.

[20] G. Litjens, O. Debats, J. Barentsz, N. Karssemeijer, and H. Huisman, "Computer-aided detection of prostate cancer in mri," *IEEE transactions on medical imaging*, vol. 33, no. 5, pp. 1083–1092, 2014.

[21] C.-C. Chang, "" libsvm: a library for support vector machines," acm transactions on intelligent systems and technology, 2: 27: 1–27: 27, 2011," *http://www. csie. ntu. edu. tw/˜ cjlin/libsvm*, vol. 2, 2011.

[22] F. Pedregosa, G. Varoquaux, A. Gramfort, V. Michel, B. Thirion, O. Grisel, M. Blondel, P. Prettenhofer, R. Weiss, V. Dubourg, *et al.*, "Scikit-learn: Machine learning in python," *Journal of machine learning research*, vol. 12, no. Oct, pp. 2825–2830, 2011.

[23] I. Chan, W. Wells, R. V. Mulkern, S. Haker, J. Zhang, K. H. Zou, S. E. Maier, and C. Tempany, "Detection of prostate cancer by integration of line-scan diffusion, t2-mapping and t2-weighted magnetic resonance imaging; a multichannel statistical classifier," *Medical physics*, vol. 30, no. 9, pp. 2390–2398, 2003.

[24] J. A. Sinnott, J. R. Rider, J. Carlsson, T. Gerke, S. Tyekucheva, K. L. Penney, H. D. Sesso, M. Loda, K. Fall, M. J. Stampfer, *et al.*, "Molecular differences in transition zone and peripheral zone prostate tumors," *Carcinogenesis*, vol. 36, no. 6, pp. 632–638, 2015.